Published online 12 May 2020

Nucleic Acids Research, 2020, Vol. 48, No. 11 **6353–6366**
doi: 10.1093/nar/gkaa337

Pby1 is a direct partner of the Dcp2 decapping enzyme

Clément Charenton [1,†], Claudine Gaudon-Plesse[2,3,4,5,†], Régis Back[1,†], Nathalie Ulryck[1], Loreline Cosson[1], Bertrand Séraphin [2,3,4,5,*] and Marc Graille [1,*]

[1]Laboratoire de Biologie Structurale de la Cellule (BIOC), CNRS, Ecole polytechnique, IP Paris, 91128 Palaiseau, France, [2]Institut de Génétique et de Biologie Moléculaire et Cellulaire (IGBMC), Illkirch, France, [3]Centre National de Recherche Scientifique (CNRS) UMR 7104, Illkirch, France, [4]Institut National de Santé et de Recherche Médicale (INSERM) U1258, Illkirch, France and [5]Université de Strasbourg, Illkirch, France

Received February 24, 2020; Revised April 17, 2020; Editorial Decision April 20, 2020; Accepted April 23, 2020

ABSTRACT

Most eukaryotic mRNAs harbor a characteristic 5′ m^{7}GpppN cap that promotes pre-mRNA splicing, mRNA nucleocytoplasmic transport and translation while also protecting mRNAs from exonucleolytic attacks. mRNA caps are eliminated by Dcp2 during mRNA decay, allowing 5′-3′ exonucleases to degrade mRNA bodies. However, the Dcp2 decapping enzyme is poorly active on its own and requires binding to stable or transient protein partners to sever the cap of target mRNAs. Here, we analyse the role of one of these partners, the yeast Pby1 factor, which is known to co-localize into P-bodies together with decapping factors. We report that Pby1 uses its C-terminal domain to directly bind to the decapping enzyme. We solved the structure of this Pby1 domain alone and bound to the Dcp1–Dcp2–Edc3 decapping complex. Structure-based mutant analyses reveal that Pby1 binding to the decapping enzyme is required for its recruitment into P-bodies. Moreover, Pby1 binding to the decapping enzyme stimulates growth in conditions in which decapping activation is compromised. Our results point towards a direct connection of Pby1 with decapping and P-body formation, both stemming from its interaction with the Dcp1–Dcp2 holoenzyme.

INTRODUCTION

Eukaryotic gene expression is a complex process initiated by transcription in the nucleus. Following their maturation, newly formed mRNAs are exported to the cytoplasm where they are translated into proteins. Simultaneously, older mRNAs are constantly degraded allowing a homeostatic maintenance of the cellular mRNA concentration.

Bulk mRNA decay is initiated by the shortening of its poly(A) tail via deadenylation, which is most often a rate-limiting and tightly regulated process (1). Shortening of the poly(A) tail is accompanied by the progressive loss of the associated poly(A) binding protein (Pab1 in yeast) that protects the mRNA 3′ end and stimulates translation. When the poly(A) tail has been shrunk to a dozen of nucleotides, Pab1 no longer binds the transcript and two alternative degradation pathways can be triggered to eliminate the mRNA body (1). The first involves severing the 5′ m^{7}GDP group from the mRNA cap, a process known as decapping, to create an entry point for 5′-3′ exonucleases such as Xrn1. The second is mediated by 3′-5′ exonucleolytic digestion of the transcript by the exosome. Both pathways initiate the recycling of released nucleotides while residual cap structures are processed by dedicated enzymes such as DcpS (2). While the scavenger activity of DcpS has been extensively described, it has also been reported to be able to cleave cap from mRNAs *in vitro* (3). The contribution of this activity to mRNA decay *in vivo* remains unclear.

Decapping is a critical step of gene expression as it blocks translation initiation and irreversibly engages the mRNA substrate in the degradation pathway. Decapping is mediated by a multimeric complex minimally composed of Dcp2, the catalytic subunit (4,5,6), and its partner Dcp1 (7). Yeast Dcp1 and Dcp2 form a stable heterodimer often referred to as the decapping holoenzyme, whereas their human counterparts require an additional subunit, EDC4 (formerly Hedls), for stable association (8). Dcp2 cleaves mRNA caps (4,5,6) through its conserved N-terminal region that consists in an N-terminal Regulatory domain (NRD), which directly binds Dcp1 and a Nudix domain that carries the catalytic residues followed by the BoxB involved in substrate binding (9). Dcp1–Dcp2 is, however, poorly active by itself, in part due to its high intrinsic flexibility (10,11,12,13,14,15) and requires several co-factors with partly redundant roles for optimal decapping activity (Pat1, Dhh1, Edc1, Edc2, Edc3 and Scd6 proteins as

*To whom correspondence should be addressed. Tel: +33 1 69 33 48 90; Fax: +33 1 69 33 49 09; Email: marc.graille@polytechnique.edu
Correspondence may also be addressed to Bertrand Séraphin. Email: seraphin@igbmc.fr
†The authors wish it to be known that, in their opinion, the first three authors should be regarded as Joint First Authors.

well as the Lsm1–7 complex in yeast and their respective homologues in other species such as PATL1, DDX6, PNRC2, EDC3, LSM14 and LSM1–7 proteins in human; (16,17,18,19,20,21,22,23,24,25,26)). Yeast Edc1 stabilizes an active conformation of Dcp1–Dcp2 in which the Dcp2-NRD domain, bound to Dcp1, and the Dcp2 Nudix domain sandwich the substrate cap to stimulate the chemistry of decapping (14,15). Edc3 enhances the affinity of Dcp2 for RNA substrates by inducing the folding of Dcp2 BoxB (11). Interestingly, the decapping activators Edc1 and Edc3 can bind simultaneously to the Dcp1–Dcp2 dimer and thus can act synergistically to stimulate decapping (15). In addition, yeast Pat1 binds (i) eight short leucine-rich helical motifs (HLM) spread along the variable C-terminal tail of Dcp2 and (ii) the Lsm1–7 complex that recognizes the 3′ end of RNA generated by deadenylation, thereby physically linking the RNAs targeted for decay to the decapping enzyme Dcp2 (17,18,27,28,29,30,31). Using an HLM present at the C-terminus of Xrn1, Pat1 also assists RNA exonucleolytic trimming following decapping (31). As proposed recently, binding of Edc3 and Pat1 to yeast Dcp2 further contributes alleviating the influence of a cis-inhibitory fragment present within its C-terminus (32,33). Besides these general mechanisms of decapping activation, specific cases of regulation of RNA decay by decapping have been identified. This includes, the regulation of the stability of the Rps28A mRNA in yeast. When an excess of the ribosomal protein Rps28 is present, it favors together with Edc3 the recruitment of the decapping complex through binding to a stem-loop structure present within its own mRNA, thereby promoting decapping independently of deadenylation (25,34,35). A related mechanism of direct recruitment of Dcp2 by Edc3 has been shown to occur for the degradation of cytoplasmic Yra1 pre-mRNA (36). Alternative modes of decapping activation, bypassing the requirement for Pat1, Edc1, Edc3 and Lsm1–7 proteins have also been shown to occur during nonsense mediated mRNA decay (NMD) where specific protein complexes encompassing Dcp1–Dcp2 have been proposed to stimulate decapping for these particular substrates (37).

At the cellular level, decapping complexes have been shown to accumulate in specific cytoplasmic foci called P-bodies that are associated with mRNAs translationally repressed and/or targeted for degradation (38,39). Controversial conclusions have been reached on whether decapping and RNA decay occur within these cellular granules (40) while experimental evidences have demonstrated that at least a fraction of decapping occurs co-translationally (41,42). The formation of P-bodies is enhanced in specific conditions such as glucose deprivation in yeast and clearly implicates partners of the decapping enzyme (43). In particular, Edc3 and the prion-like C-terminal extension of Lsm4 were proposed to play predominant roles in the formation of the protein–protein, protein–RNA and RNA–RNA networks of interactions driving the accumulation of RNA and decay factors in specific sites (44). Yet, in their absence, alternative factors such as Pby1, the RNA helicase Dhh1 and/or the RNA binding protein Psp2 were shown to mediate redundant interactions facilitating P-body formation in yeast (44).

Pby1 was reported to interact with decapping factors in several interactome studies (23,37,45,46,47,48). However, Pby1 inactivation did not impair decapping of reporter mRNAs and it was proposed to contribute to P-body assembly by destabilizing microtubules due to its similarity to the metazoan tubulin tyrosine ligase (TTL; (49)). TTL influences the stability and dynamics of microtubules by catalyzing the tyrosination of the C-terminal end of tubulin α subunit (50). A role of Pby1 in modulating P-body formation through an action on microtubules is however questionable since, unlike its mammalian homologues, yeast tubulin does not contain a C-terminal tyrosine and Pby1 does not repair the yeast alpha tubulins C-terminal ends (51). Moreover, the reported sensitivity of Pby1 to benomyl, a microtubule destabilizing drug, functionally linking it to tubulin (52), turned out to be artifactual as the gene mutated in the yeast mutant collection was not PBY1 (53). If the presence of Pby1 in P-bodies reinforced its link to decapping (49,54), its molecular function has remained elusive.

Here, we demonstrate that *Saccharomyces cerevisiae* Pby1 is a direct interaction partner of the Dcp1–Dcp2 decapping holoenzyme. Biochemical and structural analyses demonstrate that Pby1 interacts with the decapping holoenzyme through its C-terminal ATP-grasp domain, a prerequisite for Pby1 localization within P-bodies. Moreover, genetic interaction indicates that Pby1 binding to the decapping enzyme stimulates growth in conditions in which decapping activation is compromised, suggesting that Pby1 contributes to decapping activation *in vivo*.

MATERIALS AND METHODS

Pull-down assays

Pull-down experiments were performed by mixing 1 nmol of GST-*Sc*Pby1-CTD with 1 nmol of the various proteins of interest. All proteins were free of nucleic acids according to the $OD_{280\,nm}/OD_{260\,nm}$ ratio. Binding buffer (20 mM Tris–HCl pH 7.5, 150 mM NaCl, 1 mM $MgCl_2$, 10% glycerol) was added to a final volume of 60 μl. The reaction mixtures were incubated on ice for 1 h. 10 μl was withdrawn as ≪ input ≫ fraction. The remaining 50 μl were incubated with 10 μl of glutathione magnetic agarose beads (Thermo) pre-equilibrated with binding buffer in a final volume of 200 μl at 4°C for 1–1.5 h on a rotating wheel. Beads were washed three times with 500 μl of binding buffer. Bound proteins were eluted with 50 μl of elution buffer (binding buffer supplemented with 20 mM reduced glutathione). 4 μl of ≪ input ≫ and 20 μl of ≪ elution ≫ fractions were resolved on SDS-PAGE and visualized by Coomassie blue staining (or eventually silver nitrate staining).

Reconstitution, crystallization and structure determination of the Dcp1–Dcp2-[1–271]–Edc3–[2–66]–Pby1–[330–753] complex from *S. cerevisiae*

Details on cloning, expression and purification of isolated proteins as well as on structure determination of *Kl*Pby1-CTD can be found as supplementary information.

The quaternary complex formed by the Dcp1, Dcp2-[1–271], Edc3-[2–66] and Pby1-[330–753] proteins from *S. cerevisiae* was reconstituted by mixing equimolar amount of Dcp1–Dcp2-[1–271] complex and Pby1-[330–753] with an excess of Edc3-[2–66] and incubation for 30 minutes on

ice. Before injection on a Superdex 200 16/60 size exclusion column (GE Healthcare) pre-equilibrated with buffer B (20 mM Tris–HCl pH 8; 150 mM NaCl; 5 mM β-mercaptoethanol and 1 mM $MgCl_2$), the volume of the mixing reaction was adjusted to 1 ml with buffer B. The fractions corresponding to the central part of the main peak containing the four proteins of interest, were pooled and concentrated to 10 mg/ml.

Initial micro-crystals were obtained at 4°C by mixing 150 nl of quaternary complex (10 mg/ml) with an equal volume of crystallization solution (0.05 M calcium acetate; 0.1 M sodium cacodylate pH6; 25% MPD). Larger crystals were obtained within 2–3 weeks by increasing drops volume and simultaneously varying calcium acetate from 0.05 to 0.15 M and MPD from 17% to 24%. Crystals with the same morphology were obtained in the absence or the presence of ATPγS (ten-fold molar excess) but only those obtained in the presence of ATPγS led to useful datasets. Crystals were cryo-protected by transfer into the crystallization solution containing 25% MPD and ATPγS (only when crystals were grown in the presence of this nucleotide).

Several datasets were collected on beamlines Proxima-1 and Proxima-2 (Synchrotron SOLEIL, Saint-Aubin, France), ID23 and ID29 (ESRF, Grenoble, France). Data indexing and processing were performed with the program XDS (55). The best dataset was obtained by merging two datasets collected on beamline ID23 using the XSCALE program (55) and analyzed using the STARANISO server as diffraction was highly anisotropic (56). Statistics for data processing are summarized in Supplementary Table S1. The structure of the complex was solved by molecular replacement with the PHASER program using the previously solved crystal structures of *S. cerevisiae* Dcp2 Nudix domain (PDB code: 4K6E), of *Kluyveromyces lactis* Pby1 C-terminal domain (searching a first model made of domains A and C on the one side and domain B alone on the other side) and of *K. lactis* Edc3 bound to *Kl*Dcp2 region corresponding to the E3BM (11). Several cycles of building and refinement were performed using COOT (57) and BUSTER (58), respectively (see Supplementary Table S1) allowing to model some helices from *Sc*Dcp2 NRD and the N-terminal helix from *Sc*Dcp1. Due to intrinsic flexibility in the crystal, a region from *Sc*Dcp2 NRD and most of *Sc*Dcp1 could not be modeled in the $2F_o - F_c$ electron density map.

Yeast assays

For yeast growth assays, the PBY1 over-expressing plasmid (pBS4999), mutant derivatives thereof (pBS5665 and pBS5666), or control vector (pYX242; Supplementary Tables S2 and S5) were first introduced in *Δpat1/Δdhh1* and *Δpat1/Δscd6/Δedc3* yeast cells (YFW168 and BSY2601, Supplementary Table S3) by transformation. Cells were grown at the permissive temperature to the logarithmic phase in synthetic complete (SC) medium lacking leucine. Cultures were diluted to an optical density of 0.1 at 600 nm (OD_{600}) with sterile water. Three microliters of this dilution as well as 10-fold serial dilutions were plated on SC medium lacking leucine plates. Cell growth rate was monitored at 25, 30 and 34°C for the indicated time.

Two-hybrid assays

The ProQuest two-hybrid assay (Thermo) was used to monitor protein interaction. The indicated plasmids were introduced by co-transformation in strain MAV203 and transformant selected on SC medium lacking leucine and tryptophan. The β-galactosidase activity was monitored using the Beta-Glo Assay system (Promega) using cells grown in liquid SC medium lacking leucine and tryptophan. Average values and standard-error of the mean of at least two biological duplicates are plotted.

Microscopy analyses

Cells encoding a chromosomal copy of *PBY1-GFP* transformed with plasmid pBS4526 encoding EDC3-mCherry were processed as previously described (24). Briefly, after growth in SC-Leu medium at 30°C to an $OD_{600} = 0.4$, cells were shifted to the same medium lacking glucose, and incubated for 10 min at room temperature. A 1.5 ml aliquot of cells was centrifuged at 13 300 rpm for 30 s, and all but 50 μl of medium were removed. Cells were briefly vortexed, and 3 μl of suspension placed on a glass slide were immediately subjected to microscopy analysis. Imaging was performed with a Zeiss Axiovert 200M microscope attached to an Andor camera. Co-localization was performed using the GFP filter first, followed immediately by using the RFP filter. Color addition and image merging for co-localization were performed using ImageJ (59).

Additional materials and methods details are provided as supplementary information.

RESULTS

S. cerevisiae Pby1 interacts directly with the decapping machinery via its C-terminal domain

Pby1 was reported to associate with Dcp1 and Edc3 using two-hybrid assays (45,48) and to co-purify with tagged versions of these factors by affinity purification-mass spectrometry experiments (23,37,46,47). However, whether the detected interactions are direct and the region of Pby1 involved remained unclear. Sequence analyses indicate that Pby1 is a bipartite protein containing a N-terminal domain (NTD) with similarity to the SurE phosphatase family (60) and a C-terminal domain (CTD) related to the ATP-grasp fold found in TTL (Figure 1A; (50,61)). To characterize further Pby1 interaction network, we assayed the ability of full-length Pby1 or of its individual domains to interact with either Dcp1 or Edc3 using the yeast two-hybrid assay. We could reproduce earlier results when testing for the interaction between full-length Pby1 and both the Dcp1 and Edc3 proteins in *S. cerevisiae* (Figure 1A). A slightly stronger signal was observed when Pby1 was shortened to its C-terminal domain (CTD) alone while the signal was brought down to background levels for Pby1 N-terminal domain (NTD), indicating that Pby1-CTD is necessary and sufficient for these interactions.

We and others have recently shown that the association between the Edc3 and Dcp1 decapping factors is bridged by the decapping enzyme Dcp2 (11,15,62), suggesting that at least one of the interactions detected between Pby1 and

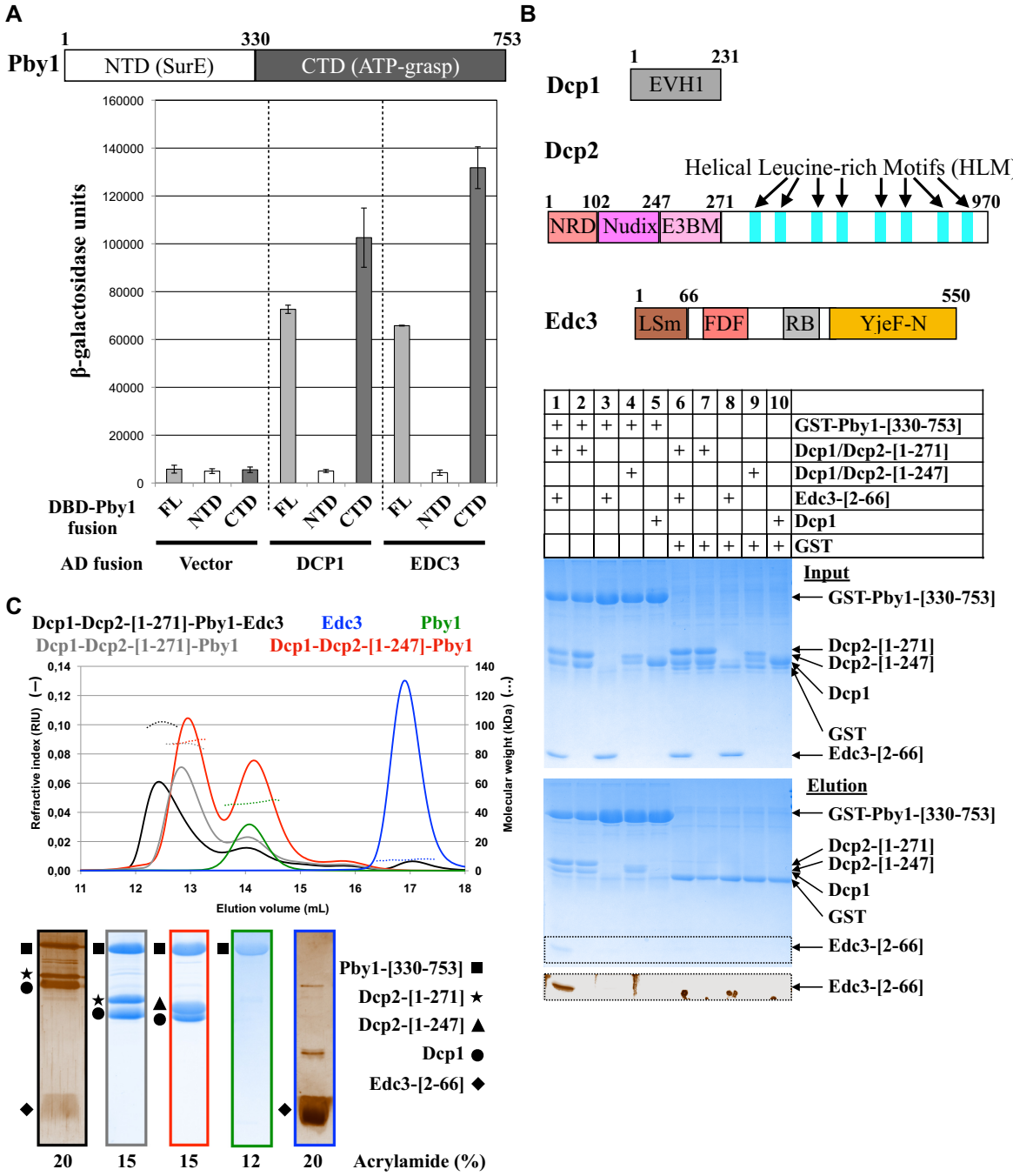

Figure 1. Pby1 interacts with the decapping machinery. (**A**) The Pby1 C-terminal domain is sufficient for interaction with both Dcp1 and Edc3 decapping factors. Schematic representation of *Saccharomyces cerevisiae* Pby1 protein. The interactions between full-length Pby1, its N- or C-terminal domains and decapping factors were studied by yeast two-hybrid assay monitoring β-galactosidase activity. Pby1 constructs were fused to the DNA binding domain (DBD) while other decapping factors (Dcp1 or Edc3) were fused to the transcription activation domain (AD). (**B**) Pby1 C-terminal domain interacts directly with the Dcp1–Dcp2 complex. Schematic representation of *Saccharomyces cerevisiae* Dcp1, Dcp2 and Edc3 proteins. EVH1: Ena/Vasp homology domain, binds Pro-rich sequences; NRD: N-terminal regulatory domain; E3BM: Edc3-binding motif; FDF: Phe-Asp-Phe motif recognized by Dhh1 helicase; RB: Rps28-binding motif; YjeF-N: Edc3 C-terminal domain forming homodimers. Pull-down experiment of various decapping complexes by GST-Pby1-CTD. Input and eluted samples were analyzed on 15% SDS/PAGE and Coomassie Blue or silver nitrate staining. (**C**) The Pby1 C-terminal domain forms stable complexes with Dcp1–Dcp2 decapping enzyme. Chromatograms resulting from SEC-MALLS analysis of the indicated proteins and/or complexes. A zoom-in centered on the main peaks with the refractive index (left y-axis; solid lines) and the distribution of molecular mass calculated from light scattering along this peak (right y-axis; dashed lines) is shown. It is noteworthy that due to an excess of Dcp1–Dcp2-[1–247] relative to Pby1-CTD, a large peak eluting at 14 mL and corresponding to Dcp1–Dcp2-[1–247] complex is visible in the analysis of the reconstituted Dcp1–Dcp2-[1–247]-Pby1-CTD complex (red curve). Coomassie Blue or silver nitrate stained SDS-PAGE analyses of the proteins present in the central fraction of the peak exhibiting the higher refractive index are shown. Gels are boxed using the same color as for the chromatograms.

both Dcp1 and Edc3 could be indirect. To assay whether Pby1 directly binds the decapping complex and identify its interaction partner, we performed an *in vitro* GST pull-down assays using purified *S. cerevisiae* proteins expressed in *E. coli*. The GST-Pby1-CTD construct specifically co-precipitated the minimal Dcp1–Dcp2-[1–271] complex in the presence of the Edc3 LSm domain (region 2–66), which is known to interact with Dcp2 through the Edc3 Binding Motif (E3BM, Dcp2-[247–260]) (compare lanes 1 and 6, Figure 1B; (11)). Next, we incubated GST-Pby1-CTD with either the Dcp1–Dcp2-[1–271] complex or Edc3 LSm but detected interaction only with Dcp1–Dcp2-[1–271] (compare lanes 2 and 3, Figure 1B). These results demonstrate that Pby1 binds directly to the decapping holoenzyme Dcp1–Dcp2 and that Edc3 is not required for this interaction. Hence, the Pby1-Edc3 interaction detected via two-hybrid is likely bridged by the Dcp1–Dcp2 complex. In line with these findings, the Dcp1–Dcp2-[1–247] complex lacking the E3BM still interacted with Pby1-CTD (lane 4; Figure 1B). We tested if Dcp1 alone could interact with Pby1-CTD (lane 5; Figure 1B) but failed to detect any interaction. Overall, our data suggest that the surface used by Pby1-CTD to bind the decapping holoenzyme is either located on Dcp2 (NRD or Nudix domain) or shared by Dcp2 and Dcp1.

Based on these findings, we used size-exclusion chromatography coupled to multi-angle laser light scattering (SEC-MALLS) to analyze both stability and oligomeric state of the identified complexes in solution. Both Edc3 LSm and Pby1-CTD in isolation showed a monomeric behavior in solution (blue and green curves, respectively, Figure 1C and Supplementary Table S4). Mixing Dcp1–Dcp2-[1–271] (grey curve) or Dcp1–Dcp2-[1–247] (red curve) complexes with a 1.2–1.5-fold molar excess of Pby1-CTD, yielded in both cases a major SEC MALLS peak corresponding to an heterotrimeric Dcp1–Dcp2–Pby1 complex as revealed by SDS-PAGE (Figure 1C) and measured molecular weight (Supplementary Table S4). Finally, when Pby1 was incubated with the Dcp1–Dcp2-[1–271]–Edc3 complex in the same conditions, the major peak (black curve, containing all four proteins according to SDS-PAGE) shifted to a smaller elution volume and showed an higher molecular weight (100 kDa) than measured for Dcp1–Dcp2-[1–271]–Pby1 (86.5 kDa) indicating the formation of an heterotetrameric Dcp1–Dcp2–Pby1–Edc3 complex. The significant shift in elution volume (0.4 mL for a theoretical molecular weight difference of 7.3 kDa) for the tetrameric complex compared to the Dcp1–Dcp2-[1–271]–Pby1 complex further indicates that the Dcp1–Dcp2–Edc3–Pby1 complex has a much larger hydrodynamic radius than the trimeric one. This observation is consistent with our crystal structure of the Dcp1–Dcp2–Edc3 complex from *K. lactis* that revealed the folding of the BoxB region of Dcp2 as a long alpha helix upon Edc3 binding (11). Altogether, this interaction data demonstrates that the C-terminal domain from Pby1 interacts directly with the Dcp1–Dcp2 complex, and indirectly with Edc3, thereby forming a heterotetrameric complex.

Pby1 C-terminal domain is a likely ATP-dependent ligase

To further characterize Pby1-CTD, we determined its crystal structure. As the *S. cerevisiae* Pby1-CTD did not crystallize, we expressed and purified the corresponding domain from various fungal orthologs. We obtained diffracting crystals for Pby1-CTD from *K. lactis* (encompassing residues 321–717; *Kl*Pby1-CTD). This structure was determined by multi-wavelength anomalous dispersion (MAD) using the anomalous signal from selenomethionine-labeled protein crystals and refined to 2.3 Å resolution to yield R and R_{free} values of 18.8% and 24%, respectively (Supplementary Table S1).

The *Kl*Pby1-CTD structure reveals the presence of three domains (Figure 2A and Supplementary Figure S1A). Domain A (residues 322–387) consists in a four stranded parallel β-sheet packed by one α-helix on each side. Domain B (residues 422–517 and 561–580) is composed of a five stranded antiparallel β-sheet with four α-helices on one side. Domain C (residues 388–421, 518–560 and 593–714) folds as a five stranded antiparallel β-sheet curved around a long central α-helix and surrounded by three α-helices. Domains A and C associate to form a large central core. These three domains and their arrangement are typical of ATP-grasp proteins (61), in agreement with predictions based on amino acid sequence analyses (49). One copy of *Kl*Pby1-CTD is present per asymmetric unit and crystal packing analysis suggests that this domain is monomeric in agreement with our SEC-MALLS experiments on *S. cerevisiae* Pby1-CTD (Figure 1C and Supplementary Table S4). Hence, Pby1-CTD differs from most ATP-grasp superfamily members such as D-alanine:D-alanine ligase, GST and LysX, which are homodimeric or tetrameric (63,64).

The comparison of *Kl*Pby1-CTD structure with known structures using the DALI server (65) reveals the highest structural similarities with *G. gallus* TTL (66), human tubulin polyglutamylase TTLL7 (TTLL stands for TTL-like; (67)) and *Xenopus tropicalis* tubulin monoglycylase TTLL3 (68) proteins with Z-score values ranging from 22.5 to 20 and rmsd values of 2–2.3Å over 160–180 Cα atoms (19–29% sequence identity, Figure 2B). As conventional ATP-grasp enzymes (61), TTL uses an ATP molecule to form an acylphosphate intermediate on the acidic group present at the C-terminal end of de-tyrosinated tubulin α subunit. This acylphosphate is then attacked by a nucleophile, the NH_2 amino group from L-tyrosine, thereby releasing phosphate and regenerating C-terminally tyrosinated tubulin α subunit (Figure 2C; (50)). Interestingly, while in most structures of ATP-grasp enzymes solved in the absence of ADP/ATP (or non-hydrolysable ATP analogues), domain B is not visible due to its flexibility, this domain is clearly defined in the $2F_o - F_c$ electron density map in our structure, despite the absence of nucleotide. This domain, which is engaged in crystal packing, adopts a position that differs from that observed for other ATP-grasp enzymes bound to nucleotides such as in the crystal structure of TTL bound to its tubulin substrate (Figure 2B; (66)). Indeed, upon nucleotide binding, domain B folds back onto domain C to clamp the nucleotide at the domains interface while, in our apo-structure of *Kl*Pby1-CTD, domain B adopts a more open confor-

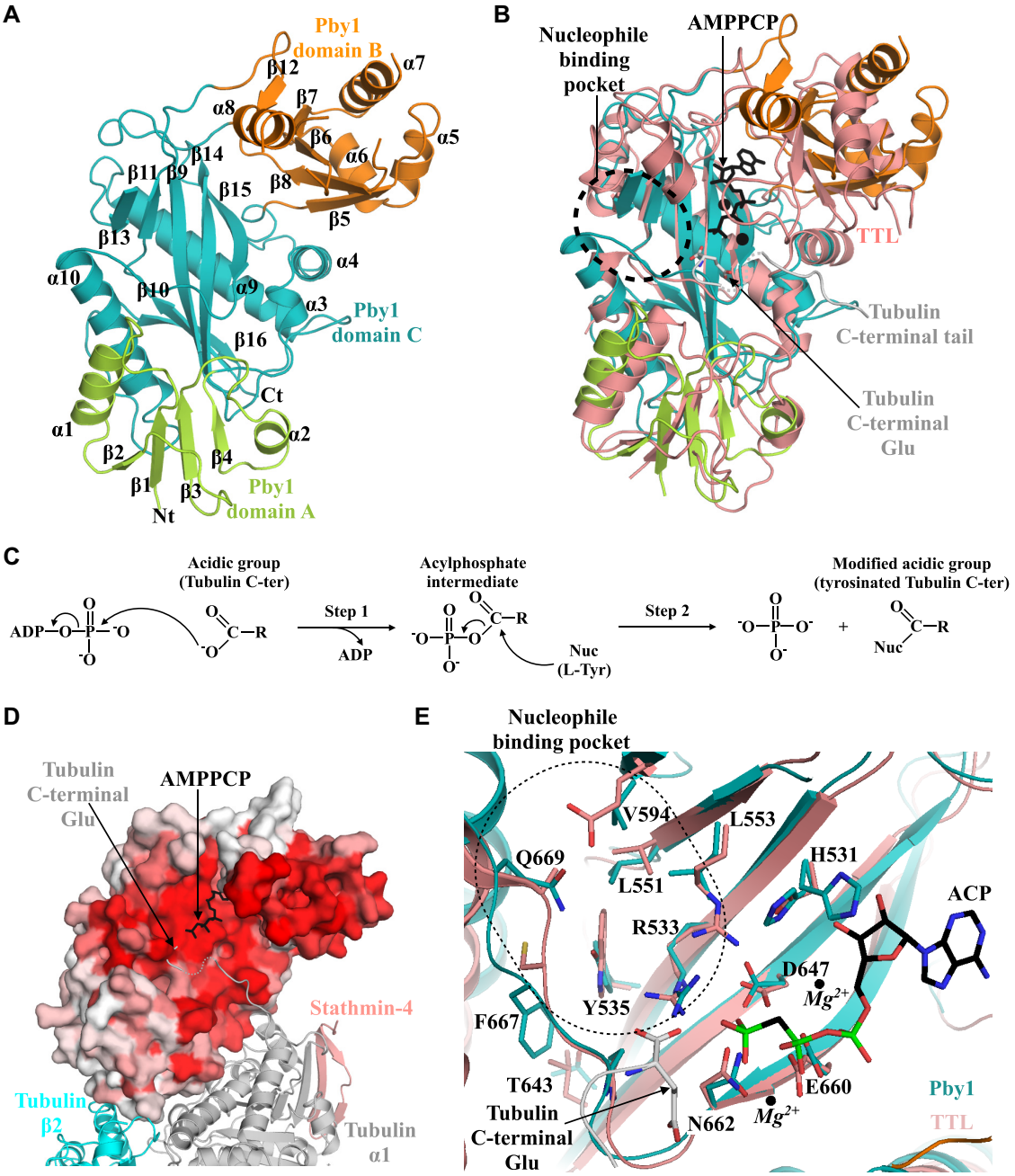

Figure 2. Structure of *Kl*Pby1-CTD. (**A**) Ribbon representation of the crystal structure of *K. lactis* Pby1 C-terminal domain. (**B**) Superimposition of *G. gallus* TTL (light pink; PDB code: 4I4T; (66)) bound to tubulin (grey) and AMPPCP (black sticks) onto *Kl*Pby1-CTD (same color code as panel A). For the sake of clarity, only the C-terminal end of tubulin (missing residues are depicted by a grey dashed line) is shown and the C-terminal glutamate from tubulin, to which a tyrosine residue is grafted, is shown as grey sticks. Two magnesium ions bound to TTL active site are shown as black spheres. The location of the nucleophile binding pocket according to other structures of ATP-grasp enzymes bound to nucleophile molecules is delineated by a black dashed circle. (**C**) Reaction mechanism catalyzed by members of the ATP-grasp ligase proteins. The acidic group and nucleophile known for the reaction catalyzed by TTL are indicated in brackets. (**D**) Mapping of the sequence conservation onto the surface of *Kl*Pby1-CTD protein structure (from no conservation in white to strict conservation in red). Conservation scores have been calculated from an alignment of fungal sequences using the Consurf server (72). The crystal structure of the TTL-tubulin-stathmin-4-AMPPCP complex has been superimposed onto *Kl*Pby1-CTD to help visualize the location of Pby1 putative active site and substrate binding pocket (66). (**E**) Comparison of TTL and *Kl*Pby1-CTD active sites and nucleophile binding pockets. Same color code as panel B. The ATP-bound conformation of *Kl*Pby1-CTD has been modeled by superimposing its different domains onto the corresponding domains from TTL in the TTL-tubulin-stathmin-4-AMPPCP complex (66). For the sake of clarity, only *Kl*Pby1-CTD residues are labeled.

mation. Hence, our structure could correspond to a preloading state ready to capture an ATP molecule for subsequent reactions.

Mapping of the sequence conservation within Pby1 orthologues onto the surface of *Kl*Pby1-CTD reveals a large and highly conserved region formed by residues from domains B and C, which matches with the regions known to interact with ATP, the nucleophile and the substrate in ATP-grasp enzymes (Figure 2D). Comparison of the *Kl*Pby1-CTD structure to that of TTL bound to tubulin (Figure 2D) reveals that the extended C-terminal tail of tubulin α1 would fit into the highly conserved region present at the surface of Pby1-CTD. This also reveals that the Pby1-CTD region matching the TTL surface interacting with the globular domain from tubulin α1 and β2, is poorly conserved. As the tubulin region facing this Pby1 area is highly conserved, this observation further reinforces the conclusion that Pby1 is not a tubulin tyrosine ligase. To compare in more details Pby1 and TTL active sites, we have superimposed the structure of TTL bound to AMPPCP, a non-hydrolyzable ATP analog and tubulin-stathmin complex to model the ATP-bound form of *Kl*Pby1-CTD (66). This reveals that the ATP binding site and the catalytic residues are conserved between both proteins (Figure 2E). In particular, the strictly conserved Glu660 from *Kl*Pby1 (Glu693 in *Sc*Pby1) matches perfectly with TTL Glu331 that interacts with a magnesium ion and which substitution by a Gln completely abolishes tubulin tyrosination activity (69). Similarly, the neighboring residues involved in the coordination of two Mg^{2+} ions in TTL active site are also conserved in Pby1 proteins (D647 and N662 in *Kl*Pby1). Finally, the side chain from *Kl*Pby1 Arg533 perfectly matches with TTL Arg202 that forms a bidentate salt bridge with the C-terminal carboxyl group from the tubulin substrate. On the contrary, most residues forming the walls of the nucleophile binding pocket differ between TTL and Pby1 (Figure 2E), strongly suggesting that L-tyrosine is not the nucleophile used by Pby1.

In conclusion, Pby1-CTD possesses all characteristics essential for catalysis by members of the ATP-grasp superfamily but significantly differs from TTL, with which it shares the strongest structural similarity. We thus propose that Pby1-CTD acts as an ATP-dependent ligase that will graft a still unknown nucleophile on the acidic group(s) of substrate(s) that remain to be identified.

Dcp2 Nudix domain binds to the Pby1–CTD putative active site

To understand how Pby1 interacts with the Dcp1–Dcp2 complex, we built-up on our SEC-MALLS results to reconstitute various Pby1-Dcp1–Dcp2 complexes by mixing Dcp1–Dcp2, Edc3 LSm domain and Pby1-CTD proteins from *S. cerevisiae* and set crystallization trials. Crystals diffracting to medium resolution and suffering from serious anisotropy could be obtained for the complex formed between Pby1-CTD, Dcp1–Dcp2-[1–271] and Edc3 LSm domain (hereafter called Dcp1–Dcp2–Edc3–Pby1 complex), yielding to a complete dataset at 3.5Å resolution (Supplementary Table S1). This structure was solved by molecular replacement using the crystal structures of each of these proteins from *S. cerevisiae* or homologs from *K. lactis* or *S. pombe*. Molecular replacement gave clear solutions for Dcp2-Nudix, Edc3 LSm and all three domains of Pby1-CTD but although an SDS-PAGE analysis confirmed the presence of the four proteins in the crystals, neither *S. cerevisiae* Dcp1 nor Dcp2-NRD structures could not be positioned by this method. Nevertheless, subsequent iterative cycles of model building and refinement, allowed modeling most of the Dcp2 NRD as well as the N-terminal α-helix from Dcp1 in the unassigned $2F_o - F_c$ and $F_o - F_c$ electron density maps. The poor quality of the map in this region indicates that the Dcp1–Dcp2 NRD module exhibits an intrinsic flexibility in the crystals, which could explain their limited and highly anisotropic diffraction. The final model was refined to 3.5 Å resolution, yielding R and R_{free} values of 24.6% and 32.1%, respectively (Figure 3A; Supplementary Table S1). During refinement of this structure, we identified a putative magnesium ion coordinated by four highly conserved acidic amino acids located within Pby1 domain B (Figure 3A). The presence of this magnesium ion is supported by: (i) its coordination sphere formed by the side chains from four conserved acidic amino acids (D446, D448, E451 and E459 according to *S. cerevisiae* numbering; Figure 3A inset and Supplementary Figure S1A); (ii) the presence of 1 mM $MgCl_2$ in the buffer used to reconstitute the Dcp1–Dcp2–Edc3–Pby1 complex and (iii) a peak in the $F_o - F_c$ electron density map resulting from the refinement of the Dcp1–Dcp2–Edc3–Pby1 structure in absence of Mg^{2+} bound to Pby1-CTD (Figure 3A). This magnesium binding site is located at the interface between Pby1 domain B and the Dcp2 Nudix domain. However, this cation is not strictly required for formation of the Dcp1–Dcp2–Edc3–Pby1 complex as this later can be formed using a buffer lacking $MgCl_2$ (data not shown). The comparison of this magnesium binding site between *Kl*Pby1 and *Sc*Pby1 crystal structures reveals that in the presence of Mg^{2+}, the side chains from E451 and to a lesser extent D446 and E459 flip towards the Mg^{2+} ion to complete the coordination sphere (Figure 3A).

In the Dcp1–Dcp2–Edc3–Pby1 complex, Edc3 LSm binds at the C-terminal end of the long α-helix (α8) formed by the BoxB protruding from Dcp2 Nudix domain as previously observed in the structures of *K. lactis* Dcp1–Dcp2–Edc3 ± Edc1 complexes (Figure 3A and Supplementary Figure S1C; (11,15)). Small differences reside in the curvature of this long Dcp2 helix, reflecting the intrinsic flexibility of this region (Supplementary Figure S2). Although only helix α1 from Dcp1 and a fraction of Dcp2 NRD are defined in the electron density maps, the interaction between Dcp1 N-terminal helix and Dcp2 NRD is also reminiscent of the interaction mode described for *S. pombe* and *K. lactis* Dcp1–Dcp2 complexes (Figure 3A and S1D; (10,11)) and will not be discussed here. Most interestingly, *S. cerevisiae* Pby1-CTD interacts almost exclusively with the Nudix domain from Dcp2 although some contacts exist between a loop located within domain A from Pby1-CTD and helices α2 and α5 from Dcp2 NRD (Figure 3A and Supplementary Figure S1B). The Pby1-Dcp2 interaction involves an ∼1200 $Å^2$ interface contributed by residues from all three Pby1 domains and by residues located in the vicinity of the Dcp2 active site (Supplementary Figure S1). Although the mod-

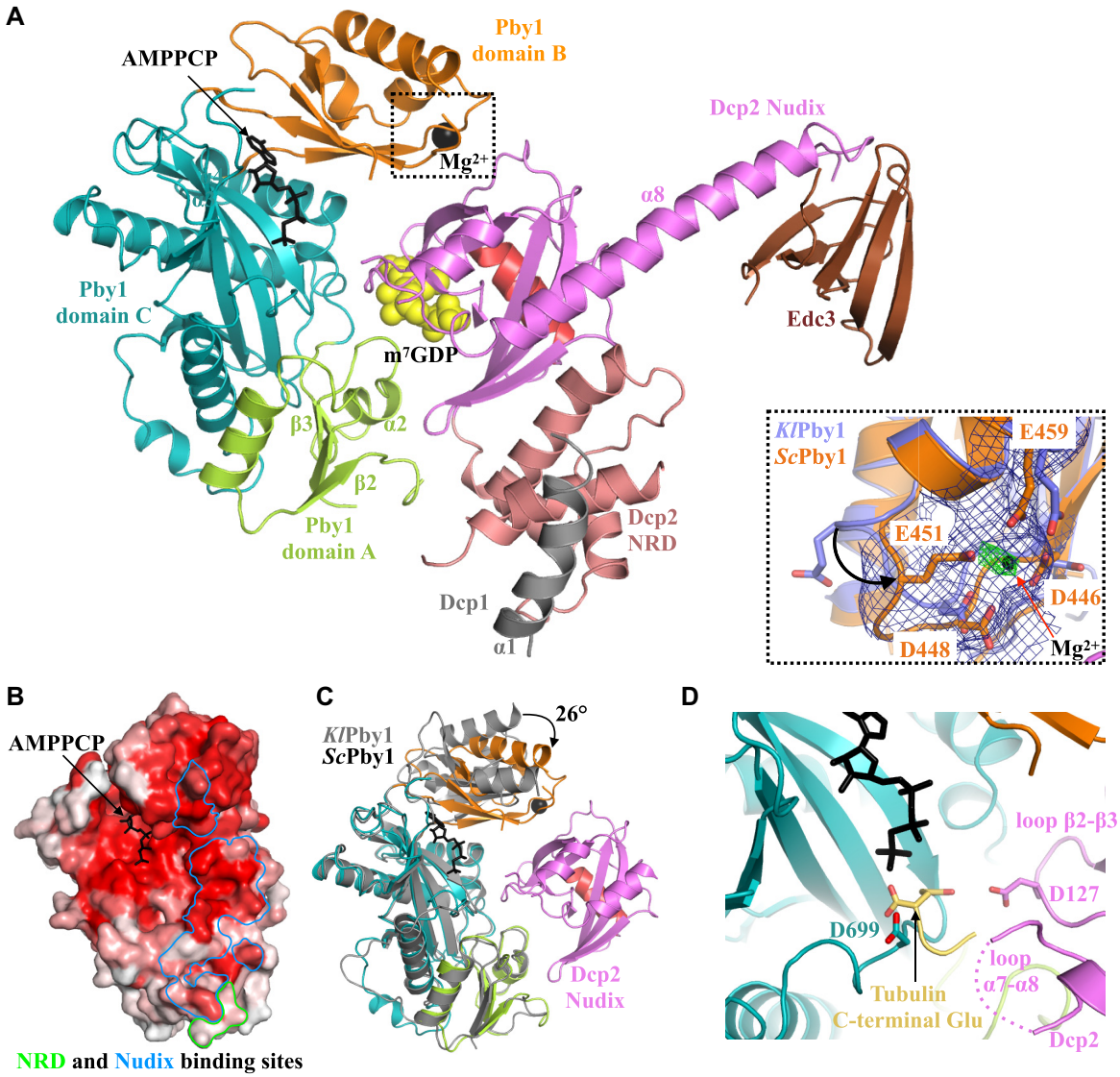

Figure 3. Pby1 interacts with the Nudix domain from Dcp2. (**A**) Ribbon representation of the crystal structure of the *S. cerevisiae* Dcp1–Dcp2–Edc3–Pby1 complex. Pby1 domains are colored using the same color code as in Figure 2A. The helix harboring the Dcp2 Nudix hydrolase signature is shown in red. A putative magnesium ion bound to Pby1 domain B is shown as a black sphere. An AMPPCP molecule, not present in our crystal structure, is shown as black sticks and has been modeled into Pby1 active site by superimposing the crystal structure of *G. gallus* TTL-tubulin-stathmin-4-AMPPCP complex (66). Similarly, a m^7GDP molecule (yellow spheres), not present in our crystal structure, has been modeled in Dcp2 active site by superimposing the structure of the *K. lactis* Dcp1–Dcp2–Edc3–m^7GDP complex (11) onto the Dcp2 Nudix domain from Dcp1–Dcp2–Edc3–Pby1 complex. For the sake of clarity, only secondary structure elements mentioned in the text are labeled. Inset: Zoom in the boxed region showing a putative Mg^{2+} binding site in Pby1 domain B. The structures of *Kl*Pby1 (light blue) and *Sc*Pby1 (orange) domains B have been superimposed. Residues involved in coordination of the Mg^{2+} ion in *Sc*Pby1 and corresponding residues in *Kl*Pby1 are shown as sticks. The $2F_o - F_c$ (contoured at 1σ) and $F_o - F_c$ (contoured at 2.5σ) electron density maps are shown in blue and green, respectively. (**B**). Dcp2 interacts with a strongly conserved region largely overlapping with the putative active site from Pby1-CTD. The sequence conservation score (calculated using the Consurf server from the same sequence alignment as for *Kl*Pby1-CTD in Figure 2D (72)) is mapped onto the surface of *Sc*Pby1-CTD protein structure (from no conservation in white to strict conservation in red). The Pby1 regions contacted by Dcp2 NRD and Nudix domain are delineated by green and blue lines, respectively. (**C**) Pby1 domain B closes onto ATP binding site in the *S. cerevisiae* Dcp1–Dcp2–Edc3–Pby1 complex. The crystal structure of *Kl*Pby1-CTD (gray) has been superimposed onto Dcp2-bound *Sc*Pby1-CTD (same color code as panel A). For the sake of clarity, Dcp1 and Edc3 have been omitted and only Dcp2 Nudix domain is shown. (**D**) Dcp2 Nudix domain is unlikely to be a Pby1 substrate. The expected location of the acidic group on which Pby1 is assumed to graft a nucleophile is visualized by superimposing the structure of TTL-Tubulin-Stathmin-AMPPCP complex (66) and corresponds to the C-terminal glutamic acid from tubulin (in yellow).

erate resolution of our crystal structure precludes a detailed analysis of the interface between Dcp2 and Pby1, it clearly reveals that Dcp2 contacts a well conserved region near Pby1 putative active site (Figure 3B). Indeed, with the exception of Pby1 residues contacting Dcp2 NRD, most Pby1 residues involved in the interaction with Dcp2 are well-conserved among Pby1 orthologues (Figure 3B and Supplementary Figure S1A). A first interaction surface is formed by residues located in the loop connecting strand β3 to helix α2 from Pby1 domain A and a crevice formed at the apical face of the Dcp2 Nudix domain. This later is localized between the m^7GDP binding site and the BoxB element, which is required for RNA binding. A second interacting area is formed by residues from Pby1 helices α3 and α4 and residues located in the vicinity of the m^7GDP binding site on Dcp2 Nudix domain. Finally, some residues proximal to the putative magnesium binding site from Pby1 domain B interact with one lateral surface of Dcp2 Nudix. This results from a 26° rotation of this Pby1 domain (relative to the large central core formed by domains A and C) upon interaction with Dcp1–Dcp2–Edc3 complex by comparison to our *Kl*Pby1-CTD structure (Figure 3C). Consequently, *Sc*Pby1-CTD, when bound to Dcp2, adopts a closed conformation reminiscent of those observed for ATP-grasp enzymes bound to ATP (or analogues) and/or substrates (66).

The binding of Dcp2 Nudix domain in the vicinity of Pby1 putative active site obviously raises the possibility that Dcp2 is Pby1′s substrate. To determine whether Dcp2 could be post-translationally modified by Pby1, similarly to tubulin by TTL and TTLLs (66,68), we superimposed the crystal structure of TTL-AMPPCP-tubulin-stathmin complex onto Pby1 in the context of the *S. cerevisiae* Dcp1–Dcp2–Edc3–Pby1 complex to locate (1) the binding sites for ATP and (2) a putative acidic group to be modified by Pby1 enzyme (Figure 3D). This reveals that the Dcp2 loops connecting strands β2 and β3 as well as helices α7 to α8 are the closest ones from Pby1 putative active site. One acidic amino acid (D127 from *S. cerevisiae* Dcp2) is present in the loop connecting strands β2 and β3 but is not conserved among Dcp2 fungal orthologues (Supplementary Figure S1A). Similarly, no conserved acidic residues are present in the loop connecting helices α7 to α8 in Dcp2 proteins. Altogether, this strongly suggests that if Pby1 is indeed an ATP-dependent ligase as indicated by its structural analysis, it is very unlikely to post-translationally modify Dcp2. Surprisingly, the side chain of D699 from *Sc*Pby1-CTD points towards the putative binding site of the acidic function to be modified by ATP-grasp enzymes (Figure 3D). This residue is strictly conserved in orthologous Pby1 proteins (Supplementary Figure S1A). Hence, we cannot exclude that in certain physiological conditions (such as glucose deprivation known to induce the formation of Pby1-containing P-bodies), Pby1 modifies D699 in *cis*, which would most probably result in its auto-inhibition. This hypothesis will have to await the detailed characterization of Pby1 biochemical function.

In conclusion, our crystal structure of the Dcp1–Dcp2–Edc3–Pby1 complex shows that Pby1-CTD interacts mainly with the Nudix domain of Dcp2 decapping enzyme and that although this later fits into the putative active site of Pby1, it is unlikely to be a Pby1 substrate.

Pby1 is recruited to P-body through its interaction with the Dcp2 Nudix domain

To validate the Dcp2–Pby1 interface observed in our structure, we substituted Pby1 residues Y409, K411 and R415 from domain C (Figure 4A) with Ala, Glu and Glu, respectively, to generate the Pby1 YKR triple mutant. GST-pull-down experiments (Figure 4B) and yeast two-hybrid assays (Figure 4C) showed that the interaction of YKR mutant with decapping factors is indeed strongly reduced both *in vitro* and *in vivo*, validating the interface observed in our crystal structure. To assess the impact of this interaction *in vivo*, we monitored the intracellular distribution of Pby1 as it was reported to co-localize with Edc3 in P-bodies upon glucose deprivation (49). Chromosomal GFP-tagged alleles expressing Pby1 and derivatives thereof were constructed to maintain protein expression at its endogenous level. Cells were transformed with a plasmid expressing Edc3–mCherry and the localization of the GFP and mCherry signals determined by microscopy with or without glucose depletion. Consistent with interaction studies (Figure 1A, B and (23,37,45,46,47,48), wild type Pby1 co-localized with Edc3–mCherry in P-bodies after glucose deprivation (Figure 4D). Using truncated Pby1 constructs, we next tested whether its N- and/or C-terminal domains behaved similarly to the full-length protein. While Pby1-CTD fused to GFP also co-localized with Edc3 in P-bodies after glucose depletion (Figure 4D), GFP-Pby1-NTD was diffusely distributed in the cytoplasm (Supplementary Figure S3). Finally, full-length Pby1 YKR mutant failed to localize in P-bodies (Figure 4D). Altogether, these data demonstrate that our structural model is biologically relevant and indicate further that Pby1 is recruited in P-bodies through its interaction with the decapping enzyme. Interestingly, P-bodies labeled with Edc3–mCherry were readily detected with GFP–Pby1–NTD or the YKR mutant, confirming that functional Pby1 is not required for their formation.

Pby1 does not impact decapping in vitro but stimulates growth in conditions in which decapping activation is compromised *in vivo*

Since its initial characterization, the Dcp1–Dcp2 decapping holoenzyme has been crystallized in many different conformations. The active form could only be trapped when bound to the m^7GDP reaction product (11,14) or with a non-hydrolyzable cap analog (15). In the absence of cap, a spectrum of orientations of the Dcp1–Dcp2 NRD module relative to the Dcp2 Nudix have been observed (10,11,12,13), indicative of a highly dynamic enzyme (Supplementary Figure S4; (9,14)). In our structure of *S. cerevisiae* Dcp1–Dcp2–Edc3–Pby1 complex, Dcp2 exhibits strong resemblance with our previously solved structure of *Kl*Dcp1–Dcp2 complex (Supplementary Figure S4A and B; (11)) and hence does not adopt an active conformation (consistent with the absence of a cap analogue in our crystallization conditions). To analyze whether Pby1-CTD could prevent Dcp2 from adopting its active conformation upon cap recognition, we superimposed the *Sc*Dcp1–Dcp2–Edc3–Pby1 and *Kl*Dcp1–Dcp2–Edc3–m^7GDP complexes onto their Dcp2 Nudix domains (Figure 5A). This reveals a potential small steric hindrance between helices α5 from Dcp2 NRD and α2

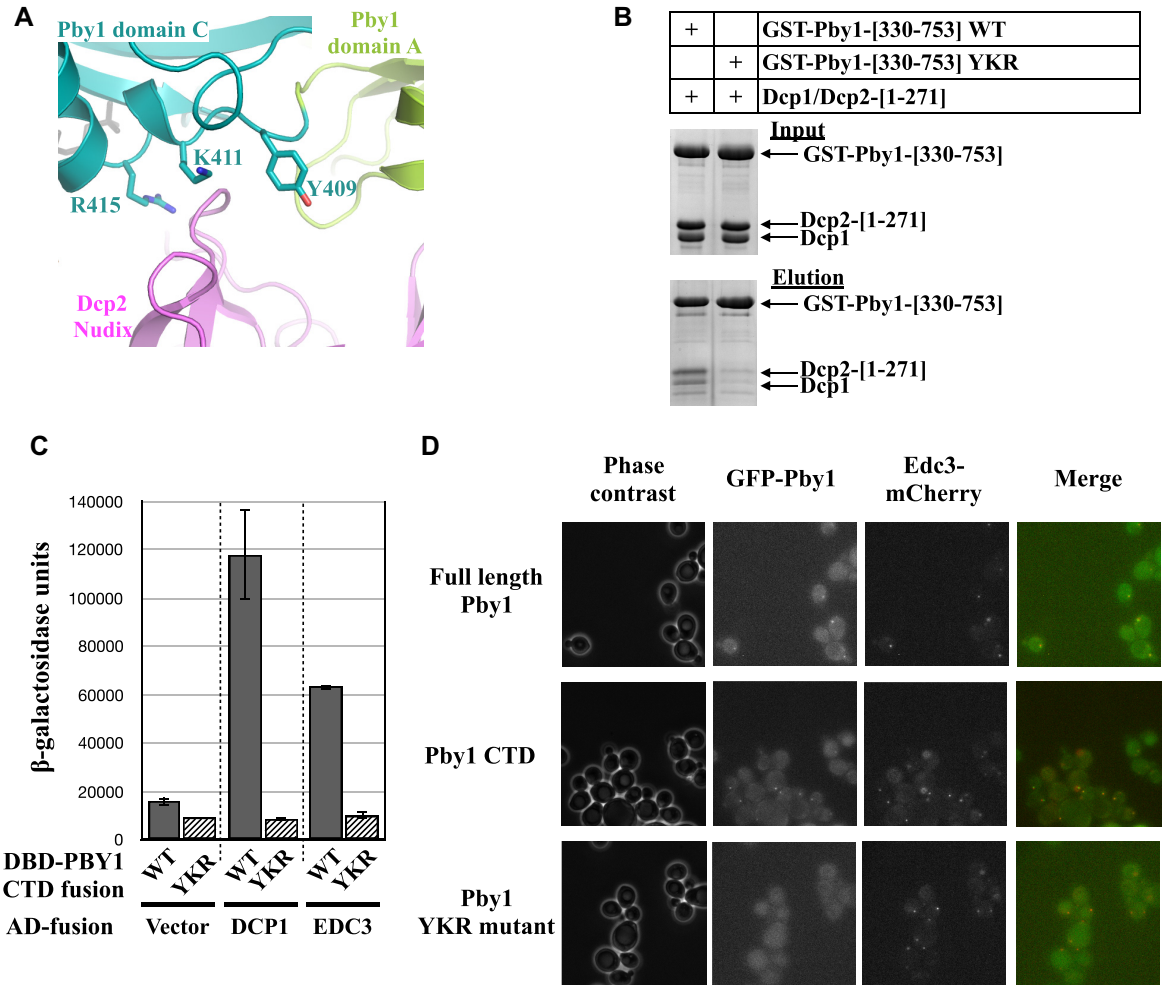

Figure 4. Preventing Pby1 to interact with Dcp2 blocks its recruitment in P-bodies. (**A**) Detailed representation of the Dcp2 binding interface involving Y409, K411 and R415 from *Sc*Pby1, which have been mutated into Ala, Glu and Glu, respectively, in the YKR mutant. Same color code as Figure 3A. (**B**). The YKR Pby1 mutant interacts loosely with the Dcp1–Dcp2 decapping complex based on GST-pull-down experiments. Input and eluted (GST pull-down) samples were analyzed on 15% SDS/PAGE and Coomassie Blue staining. (**C**). Yeast two-hybrid assay reveals that the Pby1-YKR mutant does not interacts with Dcp1 and Edc3. β-Galactosidase activity was monitored as for Figure 1A. (**D**). The C-terminal domain of Pby1 promotes its recruitment to P-bodies. Full-length and C-terminal domains of Pby1 were fused to GFP and the cellular localization was monitored by microscopy in glucose-starved cells also expressing Edc3 fused to mCherry. The YKR mutant of Pby1 was assayed alongside.

from Pby1 domain A. To probe whether this potential clash would prevent Pby1 from interacting with an activated conformation of Dcp2, we tested the impact of the m^7GpppA cap analogue, which is known to induce the switch from inactive to active conformations of the decapping enzyme, on complex formation (14,70). The Dcp1–Dcp2–Edc3 complex pre-incubated with m^7GpppA was used in GST pull-down experiments. m^7GpppA was also used in combination with a non-hydrolyzable ATP analog (ATPγS) that can either bind to Pby1–CTD or to Dcp1–Dcp2 complex (10). Neither the m^7GpppA cap analog, ATPγS nor both together affected the interaction between Pby1–CTD and the Dcp1–Dcp2–Edc3 complex (Supplementary Figure S5). We next tested whether Pby1 influenced the *in vitro* decapping activity of Dcp1–Dcp2–Edc3 and observed that Pby1 has no significant effect (neither positive nor negative; Figure 5B) on Dcp2-catalyzed decapping in our conditions. This observation, that may result from the absence of a critical cofactor in our *in vitro* reaction, prompted us to test whether Pby1 could indirectly modulate decapping *in vivo*. For this purpose, we assayed whether Pby1 over-expression could synergize or suppress the impaired growth phenotypes resulting from deletion of decapping activators. We observed that Pby1 over-expression partly suppressed the poor growth phenotype observed at 34°C after the concomitant deletion of DHH1 and PAT1 genes, two well-known decapping activators (Figure 5C; (71)). Interestingly, multi-copy suppression was also observed with a Pby1 E693Q mutant (corresponding to E660Q in *Kl*Pby1) that is assumed to obliterate the catalytic site of the ATP-grasp domain according to former studies performed on TTL E331Q mutant (Figure 5C; (69)). In contrast, the Pby1 YKR mutant was unable to suppress the Δpat1/Δdhh1 growth phenotype at 34°C, indicating that this genetic interaction requires Pby1 binding to Dcp2 (Figure 5C). Similarly, over-expressed Pby1 was also able to suppress the poor

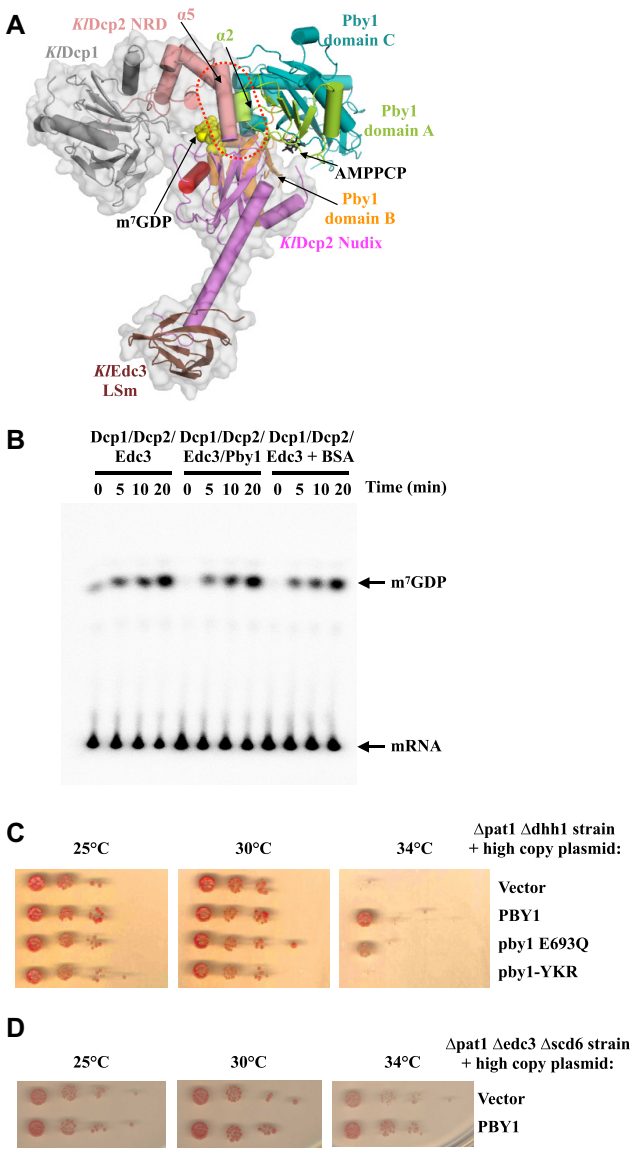

Figure 5. Pby1 interaction with Dcp2 does not affect decapping *in vitro* but suppresses poor growth in compromised decapping conditions. (**A**). The model of the interaction between Pby1 and the active form of the Dcp1–Dcp2–Edc3 decapping enzyme reveals a small steric clash (red dashed lines) between Pby1 helix α2 and Dcp2 NRD helix α5. This model was generated by superimposing Dcp2 Nudix domains from the crystal structures of *Sc*Dcp1–Dcp2–Edc3-Pby1 and *Kl*Dcp1–Dcp2–Edc3-m^{7}GDP complexes. The surface of the *Kl*Dcp1–Dcp2–Edc3–m^{7}GDP complex is shown in white. For the sake of clarity, *Sc*Dcp1, *Sc*Dcp2 and *Sc*Edc3 are not shown. Same color code as Figure 3A. (**B**). Pby1 does not affect decapping by the Dcp1–Dcp2 complex *in vitro*. Time-course reactions of decapping using a substrate with a radiolabelled cap were performed with recombinant Dcp1–Dcp2-[1–315]–Edc3-[2–200] alone or in the presence of BSA, and with Dcp1–Dcp2-[1–315]–Edc3-[2–200]–Pby1-[330–753]. The appearance of m^{7}GDP was monitored by thin layer chromatography. (C, D). Pby1 over-expression facilitates yeast growth of cells lacking several decapping activators. Yeast growth assays were performed using the *Δpat1/Δdhh1* (**C**) or *Δpat1/Δedc3/Δscd6* (**D**) strains transformed with the indicated plasmids. Serial 10-fold dilution of cultures were spotted on plates with SC medium lacking leucin and incubated at the indicated temperatures for 4 days. We would like to stress that under the same experimental conditions, the wild-type strain grows much faster that both *Δpat1/Δdhh1* or *Δpat1/Δedc3/Δscd6* strains (data not shown), in agreement with former studies (30,71).

growth of a Δpat1/Δedc3/Δscd6 yeast strain at 34°C (Figure 5D) indicating that excess Pby1 is a general suppressor of mutants affecting decapping activation rather than compensating for the deficit of a specific pathway. Overall, these observations indicate that while Pby1 does not directly modulate the Dcp2 decapping activity *in vitro* in our conditions, its interaction with the latter factor compensate for the compromised activation of decapping when it is over-expressed.

DISCUSSION

While protein–protein interaction analyses and protein localization studies assays have earlier linked Pby1 to the decapping machinery, the biological relevance of these findings remained unclear. Based on the similarity of the C-terminal domain of Pby1 to TTL and the sensitivity of a *pby1* mutant to benomyl together with the impact of tubulin mutants on P-body formation, Pby1 was proposed to contribute to P-body formation by acting on the cytoskeleton (49). Our structural analysis demonstrates that while Pby1-CTD adopts an ATP-grasp fold with high similarities to TTL (Figure 2A, B), it does not contain conserved features indicating that it could bind tubulin and/or tyrosine (Figure 2D, E). Moreover, a PBY1 deletion mutant lacking the TTL-related domain doesn't prevent P-body formation (Supplementary Figure S3). Taken together with the fact that yeast Pby1 has no detectable TTL activity *in vivo* (51) and that the reported benomyl sensitivity of *pby1* mutant (52) was incorrect (53), our data definitively argue against a role of Pby1 in modulation of P-body formation by affecting the cellular cytoskeleton.

In contrast, our structural and genetic data demonstrate that Pby1 interacts directly with Dcp2, the catalytic subunit of the decapping enzyme (Figures 1 and 3). We also show that Pby1 can associate with the Dcp1–Dcp2–Edc3 complex without clearly affecting its capacity to sever mRNA cap from transcripts *in vitro* (Figure 5B). While Pby1–CTD harbors all the required elements to catalyze the ATP-dependent transfer of a nucleophile onto an acidic group as other ATP-grasp enzymes (Figure 2E), our structure indicates that Dcp2 is unlikely to be its substrate as no conserved acidic residue lies in proximity to Pby1–CTD active site (Figure 3D). From our analysis, it remains, however, possible that Pby1 would target itself for modification (Figure 3D) but this intriguing possibility will necessitate further investigation.

At the cellular level, the binding of Pby1 through its CTD to Dcp2 promotes the recruitment of Pby1 into P-bodies (Figure 4D). Furthermore, while the Pby1-CTD is not required for P-body formation, over-expression of the full-length protein has been reported to stimulate the formation of these granules in a context where this process is genetically compromised by mutation of *edc3* and *lsm4* (44). This suggests that Pby1 might favor the clustering of the decapping enzyme in P-bodies when other factors normally performing this function, such as Edc3, are absent. This correlates with our observation that Pby1 over-expression suppressed the defective growth of yeast cells lacking several

activators of decapping (Figure 5C, D). Interestingly, while the interaction of Pby1 with the decapping enzyme is required for this function, Pby1 putative enzymatic activity (Pby1 E693Q mutant; (Figure 5C)) is not. Altogether, this suggests that Pby1 is an additional member of a long list of redundant decapping activators, encompassing Edc1/2, Edc3 and Pat1, that directly interact with Dcp2 (and in some case its Dcp1 partner) to activate decapping *in vivo*. One could hypothesize that Pby1 could for example stabilize the decapping enzyme *in vivo* or alternatively, affect its post translational modification or cellular localization. Further analyses will be necessary to uncover how Pby1 modulates decapping.

SUPPLEMENTARY DATA

Supplementary Data are available at NAR Online.

ACKNOWLEDGEMENTS

We acknowledge ESRF and SOLEIL for provision of synchrotron radiation facilities and particularly staff from Proxima-1 and Proxima-2A beamlines.
Author contributions: B.S. and M.G. designed research; C.C., C.G.P., R.B., L.C. and N.U. performed research; C.C., C.G.P., B.S. and M.G. analyzed the data and wrote the paper.

FUNDING

Ecole Polytechnique (to M.G.); Centre National pour la Recherche Scientifique (to B.S and M.G.) including a specific support by the ATIP-AVENIR program (to M.G.); Agence Nationale pour la Recherche [ANR-11-BSV800902 to B.S. and M.G., ANR-10-LABX-0030-INRT and ANR-17-EURE-0023 performed under the programme Investissements d'Avenir ANR-10-IDEX-0002-02 to B.S.]; Ligue Contre le Cancer (Equipe Labellisée 2020) (to B.S.); CERBM-IGBMC and INSERM (to B.S.); C.C. held a PhD fellowship from the French Ministère de l'Enseignement Supérieur et de la Recherche and Ecole Normale Supérieure Cachan as well as a mini post-doctoral fellowship from Ecole polytechnique. The open access publication charge for this paper has been waived by Oxford University Press – *NAR* Editorial Board members are entitled to one free paper per year in recognition of their work on behalf of the journal.
Conflict of interest statement. None declared.

REFERENCES

1. Chen,C.Y. and Shyu,A.B. (2011) Mechanisms of deadenylation-dependent decay. *Wiley Interdiscip. Rev. RNA*, **2**, 167–183.
2. Taverniti,V. and Seraphin,B. (2015) Elimination of cap structures generated by mRNA decay involves the new scavenger mRNA decapping enzyme Aph1/FHIT together with DcpS. *Nucleic Acids Res.*, **43**, 482–492.
3. Wulf,M.G., Buswell,J., Chan,S.H., Dai,N., Marks,K., Martin,E.R., Tzertzinis,G., Whipple,J.M., Correa,I.R. Jr. and Schildkraut,I. (2019) The yeast scavenger decapping enzyme DcpS and its application for in vitro RNA recapping. *Sci. Rep.*, **9**, 8594.
4. Lykke-Andersen,J. (2002) Identification of a human decapping complex associated with hUpf proteins in nonsense-mediated decay. *Mol. Cell Biol.*, **22**, 8114–8121.
5. Wang,Z., Jiao,X., Carr-Schmid,A. and Kiledjian,M. (2002) The hDcp2 protein is a mammalian mRNA decapping enzyme. *Proc. Natl. Acad. Sci. U.S.A.*, **99**, 12663–12668.
6. van Dijk,E., Cougot,N., Meyer,S., Babajko,S., Wahle,E. and Seraphin,B. (2002) Human Dcp2: a catalytically active mRNA decapping enzyme located in specific cytoplasmic structures. *EMBO J.*, **21**, 6915–6924.
7. Beelman,C.A., Stevens,A., Caponigro,G., LaGrandeur,T.E., Hatfield,L., Fortner,D.M. and Parker,R. (1996) An essential component of the decapping enzyme required for normal rates of mRNA turnover. *Nature*, **382**, 642–646.
8. Fenger-Gron,M., Fillman,C., Norrild,B. and Lykke-Andersen,J. (2005) Multiple processing body factors and the ARE binding protein TTP activate mRNA decapping. *Mol. Cell*, **20**, 905–915.
9. Charenton,C. and Graille,M. (2018) mRNA decapping: finding the right structures. *Philos. Trans. Roy. Soc. Lond. B, Biol. Sci.*, **373**, 20180164.
10. She,M., Decker,C.J., Svergun,D.I., Round,A., Chen,N., Muhlrad,D., Parker,R. and Song,H. (2008) Structural basis of dcp2 recognition and activation by dcp1. *Mol. Cell*, **29**, 337–349.
11. Charenton,C., Taverniti,V., Gaudon-Plesse,C., Back,R., Seraphin,B. and Graille,M. (2016) Structure of the active form of Dcp1–Dcp2 decapping enzyme bound to m7GDP and its Edc3 activator. *Nat. Struct. Mol. Biol.*, **23**, 982–986.
12. Mugridge,J.S., Ziemniak,M., Jemielity,J. and Gross,J.D. (2016) Structural basis of mRNA-cap recognition by Dcp1–Dcp2. *Nat. Struct. Mol. Biol.*, **23**, 987–994.
13. Valkov,E., Muthukumar,S., Chang,C.T., Jonas,S., Weichenrieder,O. and Izaurralde,E. (2016) Structure of the Dcp2-Dcp1 mRNA-decapping complex in the activated conformation. *Nat. Struct. Mol. Biol.*, **23**, 574–579.
14. Wurm,J.P., Holdermann,I., Overbeck,J.H., Mayer,P.H.O. and Sprangers,R. (2017) Changes in conformational equilibria regulate the activity of the Dcp2 decapping enzyme. *Proc. Natl. Acad. Sci. U.S.A.*, **114**, 6034–6039.
15. Mugridge,J.S., Tibble,R.W., Ziemniak,M., Jemielity,J. and Gross,J.D. (2018) Structure of the activated Edc1-Dcp1–Dcp2–Edc3 mRNA decapping complex with substrate analog poised for catalysis. *Nat. Commun.*, **9**, 1152.
16. Bonnerot,C., Boeck,R. and Lapeyre,B. (2000) The two proteins Pat1p (Mrt1p) and Spb8p interact in vivo, are required for mRNA decay, and are functionally linked to Pab1p. *Mol. Cell. Biol.*, **20**, 5939–5946.
17. Bouveret,E., Rigaut,G., Shevchenko,A., Wilm,M. and Seraphin,B. (2000) A Sm-like protein complex that participates in mRNA degradation. *EMBO J.*, **19**, 1661–1671.
18. Tharun,S., He,W., Mayes,A.E., Lennertz,P., Beggs,J.D. and Parker,R. (2000) Yeast Sm-like proteins function in mRNA decapping and decay. *Nature*, **404**, 515–518.
19. Coller,J.M., Tucker,M., Sheth,U., Valencia-Sanchez,M.A. and Parker,R. (2001) The DEAD box helicase, Dhh1p, functions in mRNA decapping and interacts with both the decapping and deadenylase complexes. *RNA (New York, N.Y.)*, **7**, 1717–1727.
20. Dunckley,T., Tucker,M. and Parker,R. (2001) Two related proteins, Edc1p and Edc2p, stimulate mRNA decapping in Saccharomyces cerevisiae. *Genetics*, **157**, 27–37.
21. Fischer,N. and Weis,K. (2002) The DEAD box protein Dhh1 stimulates the decapping enzyme Dcp1. *EMBO J.*, **21**, 2788–2797.
22. Kshirsagar,M. and Parker,R. (2004) Identification of Edc3p as an enhancer of mRNA decapping in Saccharomyces cerevisiae. *Genetics*, **166**, 729–739.
23. Decourty,L., Saveanu,C., Zemam,K., Hantraye,F., Frachon,E., Rousselle,J.C., Fromont-Racine,M. and Jacquier,A. (2008) Linking functionally related genes by sensitive and quantitative characterization of genetic interaction profiles. *Proc. Natl. Acad. Sci. U.S.A.*, **105**, 5821–5826.
24. Nissan,T., Rajyaguru,P., She,M., Song,H. and Parker,R. (2010) Decapping activators in Saccharomyces cerevisiae act by multiple mechanisms. *Mol. Cell*, **39**, 773–783.
25. Kolesnikova,O., Back,R., Graille,M. and Seraphin,B. (2013) Identification of the Rps28 binding motif from yeast Edc3 involved in

the autoregulatory feedback loop controlling RPS28B mRNA decay. *Nucleic. Acids. Res.*, **41**, 9514–9523.
26. He,F., Celik,A., Wu,C. and Jacobson,A. (2018) General decapping activators target different subsets of inefficiently translated mRNAs. *eLife*, **7**, e34409.
27. Chowdhury,A., Mukhopadhyay,J. and Tharun,S. (2007) The decapping activator Lsm1p-7p-Pat1p complex has the intrinsic ability to distinguish between oligoadenylated and polyadenylated RNAs. *RNA (New York, N.Y.)*, **13**, 998–1016.
28. Sharif,H. and Conti,E. (2013) Architecture of the lsm1-7-pat1 complex: a conserved assembly in eukaryotic mRNA turnover. *Cell Rep.*, **5**, 283–291.
29. Wu,D., Muhlrad,D., Bowler,M.W., Liu,Z., Parker,R. and Song,H. (2013) Lsm2 and Lsm3 bridge the interaction of the Lsm1-7 complex with Pat1 for decapping activation. *Cell Res.*, **24**, 233–246.
30. Fourati,Z., Kolesnikova,O., Back,R., Keller,J., Charenton,C., Taverniti,V., Plesse,C.G., Lazar,N., Durand,D., van Tilbeurgh,H *et al.*2014) The C-terminal domain from S. cerevisiae Pat1 displays two conserved regions involved in decapping factor recruitment. *PLoS One*, **9**, e96828.
31. Charenton,C., Gaudon-Plesse,C., Fourati,Z., Taverniti,V., Back,R., Kolesnikova,O., Seraphin,B. and Graille,M. (2017) A unique surface on Pat1 C-terminal domain directly interacts with Dcp2 decapping enzyme and Xrn1 5′-3′ mRNA exonuclease in yeast. *Proc. Natl. Acad. Sci. U.S.A.*, **114**, E9493–E9501.
32. He,F. and Jacobson,A. (2015) Control of mRNA decapping by positive and negative regulatory elements in the Dcp2 C-terminal domain. *RNA (New York, N.Y.)*, **21**, 1633–1647.
33. Paquette,D.R., Tibble,R.W., Daifuku,T.S. and Gross,J.D. (2018) Control of mRNA decapping by autoinhibition. *Nucleic Acids Res.*, **46**, 6318–6329.
34. Badis,G., Saveanu,C., Fromont-Racine,M. and Jacquier,A. (2004) Targeted mRNA degradation by deadenylation-independent decapping. *Mol. Cell*, **15**, 5–15.
35. Harigaya,Y., Jones,B.N., Muhlrad,D., Gross,J.D. and Parker,R. (2010) Identification and analysis of the interaction between Edc3 and Dcp2 in Saccharomyces cerevisiae. *Mol. Cell. Biol.*, **30**, 1446–1456.
36. Dong,S., Jacobson,A. and He,F. (2010) Degradation of YRA1 Pre-mRNA in the cytoplasm requires translational repression, multiple modular intronic elements, Edc3p, and Mex67p. *PLoS Biol.*, **8**, e1000360.
37. Dehecq,M., Decourty,L., Namane,A., Proux,C., Kanaan,J., Le Hir,H., Jacquier,A. and Saveanu,C. (2018) Nonsense-mediated mRNA decay involves two distinct Upf1-bound complexes. *EMBO J.*, **37**, e99278.
38. Sheth,U. and Parker,R. (2003) Decapping and decay of messenger RNA occur in cytoplasmic processing bodies. *Science*, **300**, 805–808.
39. Cougot,N., Babajko,S. and Seraphin,B. (2004) Cytoplasmic foci are sites of mRNA decay in human cells. *J. Cell Biol.*, **165**, 31–40.
40. Horvathova,I., Voigt,F., Kotrys,A.V., Zhan,Y., Artus-Revel,C.G., Eglinger,J., Stadler,M.B., Giorgetti,L. and Chao,J.A. (2017) The dynamics of mRNA turnover revealed by single-molecule imaging in single cells. *Mol. Cell*, **68**, 615–625.
41. Hu,W., Sweet,T.J., Chamnongpol,S., Baker,K.E. and Coller,J. (2009) Co-translational mRNA decay in Saccharomyces cerevisiae. *Nature*, **461**, 225–229.
42. Pelechano,V., Wei,W. and Steinmetz,L.M. (2015) Widespread Co-translational RNA decay reveals ribosome dynamics. *Cell*, **161**, 1400–1412.
43. Jonas,S. and Izaurralde,E. (2013) The role of disordered protein regions in the assembly of decapping complexes and RNP granules. *Genes Dev.*, **27**, 2628–2641.
44. Rao,B.S. and Parker,R. (2017) Numerous interactions act redundantly to assemble a tunable size of P bodies in Saccharomyces cerevisiae. *Proc. Natl. Acad. Sci. U.S.A.*, **114**, E9569–E9578.
45. Ito,T., Chiba,T., Ozawa,R., Yoshida,M., Hattori,M. and Sakaki,Y. (2001) A comprehensive two-hybrid analysis to explore the yeast protein interactome. *Proc. Natl. Acad. Sci. U.S.A.*, **98**, 4569–4574.
46. Gavin,A.C., Aloy,P., Grandi,P., Krause,R., Boesche,M., Marzioch,M., Rau,C., Jensen,L.J., Bastuck,S., Dumpelfeld,B. *et al.* (2006) Proteome survey reveals modularity of the yeast cell machinery. *Nature*, **440**, 631–636.
47. Krogan,N.J., Cagney,G., Yu,H., Zhong,G., Guo,X., Ignatchenko,A., Li,J., Pu,S., Datta,N., Tikuisis,A.P. *et al.* (2006) Global landscape of protein complexes in the yeast Saccharomyces cerevisiae. *Nature*, **440**, 637–643.
48. Yu,H., Braun,P., Yildirim,M.A., Lemmens,I., Venkatesan,K., Sahalie,J., Hirozane-Kishikawa,T., Gebreab,F., Li,N., Simonis,N. *et al.* (2008) High-quality binary protein interaction map of the yeast interactome network. *Science*, **322**, 104–110.
49. Sweet,T.J., Boyer,B., Hu,W., Baker,K.E. and Coller,J. (2007) Microtubule disruption stimulates P-body formation. *RNA (New York, N.Y.)*, **13**, 493–502.
50. Nieuwenhuis,J. and Brummelkamp,T.R. (2019) The Tubulin Detyrosination Cycle: Function and Enzymes. *Trends Cell Biol.*, **29**, 80–92.
51. Badin-Larcon,A.C., Boscheron,C., Soleilhac,J.M., Piel,M., Mann,C., Denarier,E., Fourest-Lieuvin,A., Lafanechere,L., Bornens,M. and Job,D. (2004) Suppression of nuclear oscillations in Saccharomyces cerevisiae expressing Glu tubulin. *Proc. Natl. Acad. Sci. U.S.A.*, **101**, 5577–5582.
52. Parsons,A.B., Brost,R.L., Ding,H., Li,Z., Zhang,C., Sheikh,B., Brown,G.W., Kane,P.M., Hughes,T.R. and Boone,C. (2004) Integration of chemical-genetic and genetic interaction data links bioactive compounds to cellular target pathways. *Nat. Biotechnol.*, **22**, 62–69.
53. Olmezer,G., Klein,D. and Rass,U. (2015) DNA repair defects ascribed to pby1 are caused by disruption of Holliday junction resolvase Mus81-Mms4. *DNA Repair (Amst.)*, **33**, 17–23.
54. Denervaud,N., Becker,J., Delgado-Gonzalo,R., Damay,P., Rajkumar,A.S., Unser,M., Shore,D., Naef,F. and Maerkl,S.J. (2013) A chemostat array enables the spatio-temporal analysis of the yeast proteome. *Proc. Natl. Acad. Sci. U.S.A.*, **110**, 15842–15847.
55. Kabsch,W. (2010) Xds. *Acta Crystallogr. D. Biol. Crystallogr.*, **66**, 125–132.
56. Tickle,I.J., Flensburg,C., Keller,P., Paciorek,W., Sharff,A., Vonrhein,C. and Bricogne,G. (2018) Global Phasing Ltd, Cambridge.
57. Emsley,P., Lohkamp,B., Scott,W.G. and Cowtan,K. (2010) Features and development of Coot. *Acta Crystallogr. D. Biol. Crystallogr.*, **66**, 486–501.
58. Bricogne,G., Blanc,E., Brandl,M., Flensburg,C., Keller,P., Paciorek,W., Roversi,P., Sharff,A., Smart,O.S., Vonrhein,C. *et al.* (2016) Global Phasing Ltd, Cambridge.
59. Schneider,C.A., Rasband,W.S. and Eliceiri,K.W. (2012) NIH Image to ImageJ: 25 years of image analysis. *Nat. Methods*, **9**, 671–675.
60. Iwasaki,W. and Miki,K. (2007) Crystal structure of the stationary phase survival protein SurE with metal ion and AMP. *J. Mol. Biol.*, **371**, 123–136.
61. Fawaz,M.V., Topper,M.E. and Firestine,S.M. (2011) The ATP-grasp enzymes. *Bioorg. Chem.*, **39**, 185–191.
62. Fromm,S.A., Truffault,V., Kamenz,J., Braun,J.E., Hoffmann,N.A., Izaurralde,E. and Sprangers,R. (2012) The structural basis of Edc3- and Scd6-mediated activation of the Dcp1:Dcp2 mRNA decapping complex. *EMBO J.*, **31**, 279–290.
63. Fan,C., Moews,P.C., Shi,Y., Walsh,C.T. and Knox,J.R. (1995) A common fold for peptide synthetases cleaving ATP to ADP: glutathione synthetase and D-alanine:d-alanine ligase of Escherichia coli. *Proc. Natl. Acad. Sci. U.S.A.*, **92**, 1172–1176.
64. Sakai,H., Vassylyeva,M.N., Matsuura,T., Sekine,S., Gotoh,K., Nishiyama,M., Terada,T., Shirouzu,M., Kuramitsu,S., Vassylyev,D.G. *et al.* (2003) Crystal structure of a lysine biosynthesis enzyme, LysX, from Thermus thermophilus HB8. *J. Mol. Biol.*, **332**, 729–740.
65. Holm,L. and Laakso,L.M. (2016) Dali server update. *Nucleic. Acids. Res.*, **44**, W351–W355.
66. Prota,A.E., Bargsten,K., Zurwerra,D., Field,J.J., Diaz,J.F., Altmann,K.H. and Steinmetz,M.O. (2013) Molecular mechanism of action of microtubule-stabilizing anticancer agents. *Science*, **339**, 587–590.
67. Garnham,C.P., Vemu,A., Wilson-Kubalek,E.M., Yu,I., Szyk,A., Lander,G.C., Milligan,R.A. and Roll-Mecak,A. (2015) Multivalent microtubule recognition by tubulin tyrosine ligase-like family glutamylases. *Cell*, **161**, 1112–1123.
68. Garnham,C.P., Yu,I., Li,Y. and Roll-Mecak,A. (2017) Crystal structure of tubulin tyrosine ligase-like 3 reveals essential architectural elements unique to tubulin monoglycylases. *Proc. Natl. Acad. Sci. U.S.A.*, **114**, 6545–6550.

69. Szyk,A., Deaconescu,A.M., Piszczek,G. and Roll-Mecak,A. (2011) Tubulin tyrosine ligase structure reveals adaptation of an ancient fold to bind and modify tubulin. *Nat. Struct. Mol. Biol.*, **18**, 1250–1258.
70. Floor,S.N., Jones,B.N., Hernandez,G.A. and Gross,J.D. (2010) A split active site couples cap recognition by Dcp2 to activation. *Nat. Struct. Mol. Biol.*, **17**, 1096–1101.
71. Balagopal,V. and Parker,R. (2009) Stm1 modulates mRNA decay and Dhh1 function in Saccharomyces cerevisiae. *Genetics*, **181**, 93–103.
72. Ashkenazy,H., Erez,E., Martz,E., Pupko,T. and Ben-Tal,N. (2010) ConSurf 2010: calculating evolutionary conservation in sequence and structure of proteins and nucleic acids. *Nucleic. Acids. Res.*, **38**, W529–W533.